A Novel Lung Cancer Signature Mediates Metastatic Bone Colonization by a Dual Mechanism

Silvestre Vicent,[1] Diego Luis-Ravelo,[1] Iker Antón,[1] Ignacio García-Tuñón,[1] Francisco Borrás-Cuesta,[2] Javier Dotor,[3] Javier De Las Rivas,[4] and Fernando Lecanda[1]

[1]Division of Oncology, Adhesion and Metastasis Laboratory and [2]Division of Hepatology and Gene Therapy, Center for Applied Medical Research, University of Navarra, Pamplona, Spain; [3]Digna Biotech, Madrid, Spain; and [4]Bioinformatics and Functional Genomics Research Group, Cancer Research Center, University of Salamanca, Salamanca, Spain

Abstract

Bone is a frequent target of lung cancer metastasis, which is associated with significant morbidity and a dismal prognosis. To identify and functionally characterize genes involved in the mechanisms of osseous metastasis, we developed a murine lung cancer model. Comparative transcriptomic analysis identified genes encoding signaling molecules (such as *TCF4* and *PRKD3*) and cell anchorage–related proteins (*MCAM* and *SUSD5*), some of which were basally modulated by transforming growth factor-β (TGF-β) in tumor cells and in conditions mimicking tumor-stromal interactions. Triple gene combinations induced not only high osteoclastogenic activity but also a marked enhancement of global metalloproteolytic activities *in vitro*. These effects were strongly associated with robust bone colonization *in vivo*, whereas this gene subset was ineffective in promoting local tumor growth and cell homing activity to bone. Interestingly, global inhibition of metalloproteolytic activities and simultaneous TGF-β blockade *in vivo* led to increased survival and a remarkable attenuation of bone tumor burden and osteolytic metastasis. Thus, this metastatic gene signature mediates bone matrix degradation by a dual mechanism of induction of TGF-β–dependent osteoclastogenic bone resorption and enhancement of stroma-dependent metalloproteolytic activities. Our findings suggest the cooperative contribution of host-derived and cell autonomous effects directed by a small subset of genes in mediating aggressive osseous colonization. [Cancer Res 2008;68(7):2275–85]

Introduction

Lung cancer is the leading cause of mortality in Western countries, causing more than 500,000 deaths per year in the United States and more than 1 million deaths per year worldwide. The 5-year survival rate is around 10% to 15% (1).

Lung cancer is classified into two major groups: non–small cell lung carcinoma (NSCLC), which accounts for 75% of all cases, and SCLC, which accounts for ~25% of lung neoplasms. NSCLC is divided into three histologic subtypes: adenocarcinoma (30–40%), squamous cell carcinoma (20–25%), and large cell carcinoma (15–20%; ref. 2). Large cell carcinoma, which represents the fourth most frequent of the histologic varieties, is strongly associated with tobacco smoking (3) and is the most lethal of all NSCLC subtypes, with a 5-year survival rate of <7% (4).

Most of the current efforts aimed to ameliorate lung cancer are based on early diagnostic modalities and new therapies. However, there are few studies dealing with metastases, the most devastating complication of lung cancer that is responsible for ~90% of deaths. Despite the fact that stage I disease is associated with a favorable prognosis, ~30% of NSCLC patients diagnosed with stage I disease develop metastasis after complete tumor resection (5). Lung cancer cells often escape from primary sites and tend to spread locally in the thoracic cavity, including the pleural space, as well as in distant organs, including the brain, the skeleton, adrenals, pericardium, and liver (6). Bone, a fertile "soil" for tumor cells (7), is a frequent site of lung metastasis and as many as 30% to 40% of patients with NSCLC have bone metastases (8, 9). Patients with bone metastases experience significant morbidity, including pain, hypercalcemia of malignancy, and spinal cord compression associated with pathologic fractures frequently impairing mobility (9). All of these skeletal-related events entail a significant reduction in quality of life, decrease survival (9), and require costly treatment (10).

It has long been recognized that bone provides a favorable environment for tumor cell homing and colonization because it is a major reservoir of growth factors, such as transforming growth factor-β (TGF-β) and insulin-like growth factor. In several tumors, TGF-β has been shown to promote the growth of bone metastasis (11, 12), whereas in normal epithelia and low-grade tumors TGF-β acts as potent growth inhibitor (13, 14). In most of the studies performed in breast cancer, blockade of TGF-β signaling either by a stable knockdown of SMAD4 (15, 16) or by a dominant-negative approach decreased bone metastatic lesions and dramatically reduced the tumor burden and osteolytic metastases (17, 18). These lesions were associated with a marked increase in osteoclastic activation induced by tumor-derived parathyroid hormone-related protein (PTHrP; refs. 17, 19). For breast cancer, these findings establish that in the bone microenvironment tumor release factors stimulate osteoclast resorption, which contribute to bone matrix degradation. In turn, this process liberates active TGF-β from the bone matrix, which fuels tumor cells to secrete PTHrP and other osteoclastogenic factors, and thus creates a perpetuated "vicious cycle" implicated in osteolytic lesions (12, 20). However, to what extent the same paradigm of breast cancer metastasis applies to lung cancer dissemination to bone or involves other complementary mechanisms of colonization remains to be explored.

The variety of lung histologic subtypes is in contrast to the paucity of experimental models of osseous lung metastasis

Note: Supplementary data for this article are available at Cancer Research Online (http://cancerres.aacrjournals.org/).

Current address for S. Vicent: Division of Hematology/Oncology, Department of Pediatrics, Stanford University, Stanford, California.

Requests for reprints: Fernando Lecanda, Center for Applied Medical Research, University of Navarra, 31080 Pamplona, Spain. Phone: 34-948-194-700; Fax: 34-948-194-714; E-mail: flecanda@unav.es.

doi:10.1158/0008-5472.CAN-07-6493

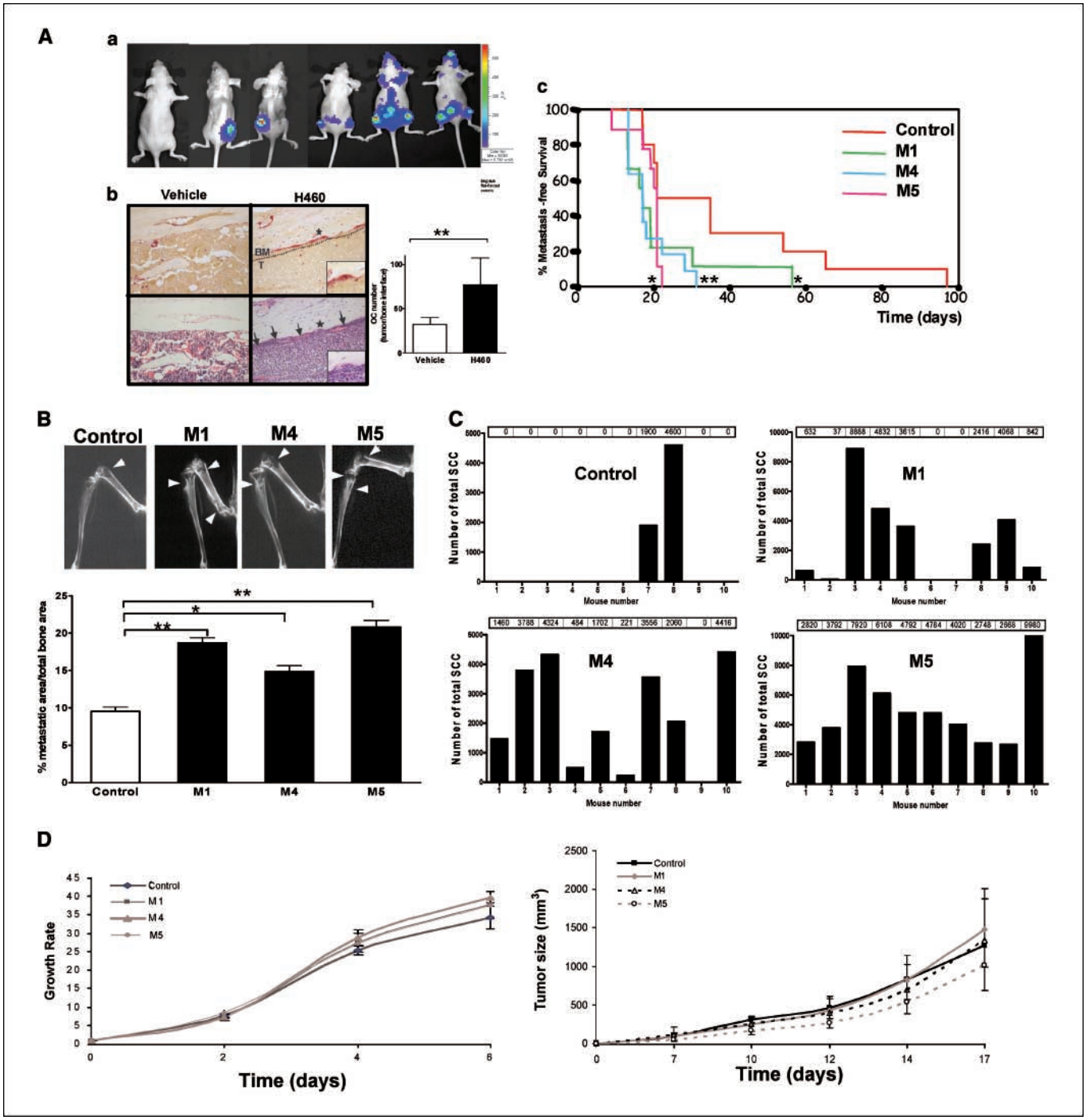

Figure 1. Selection of highly metastatic subpopulations in a model of lung cancer metastasis to bone. *A, a,* nude mice were inoculated with H460 cell line by i.c. injection and monitored using bioluminescence imaging. Twenty to 30 d after inoculation, H460 cells were found in the hind limbs, spine, and fore limbs. *b,* TRAP-stained section shows numerous osteoclasts covering the endosteal surface of the femoral diaphysis (*arrows*). *BM,* bone marrow; *T,* tumor cells. *Star,* area of the inset in two serial sections. *Lower panels*, serial H&E-stained section after i.c. inoculation with H460 cells or vehicle alone. The number of osteoclasts at the tumor-bone interface was counted and compared with vehicle-inoculated animals. *Columns,* mean of eight mice per group; *bars,* SE. **, $P < 0.01$. *c,* Kaplan-Meier curves showing the metastasis-free survival of mice inoculated with control cells (H460) and various *in vivo* selected subpopulations (*M1, M4,* and *M5*). Nude mice were i.c. inoculated with the H460 control cell line. Several subpopulations (M1, M4, and M5 and others included in Supplementary Fig. S1) were isolated, expanded in culture, and i.c. reinoculated (10 mice per group). *B,* X-ray image analysis of the metastatic area 22 d after inoculation. *C,* 20 d after i.c. inoculation of control and M1, M4, and M5 subpopulations, SCCs were isolated from the hind limbs, grown for 5 d *in vitro*, and counted. *D,* proliferation rate *in vitro* by 3-(4,5-dimethylthiazol-2-yl)-2,5-diphenyltetrazolium bromide at 2, 4, and 6 d (*left*) and s.c. tumor growth *in vivo* (*right*). No differences in *in vitro* proliferation or *in vivo* s.c. tumor growth were found. *Points,* mean; *bars,* SE. *, $P < 0.05$; **, $P < 0.01$.

available. Thus, to elucidate the molecular mechanisms of bone metastasis, we screened a large battery of cell lines from different tumor subtypes. In this report, we selected one model of large cell carcinoma characterized by its ability to induce the most aggressive osseous lesions. Using global transcriptomic analysis, the genetic program mediating this process was investigated. A novel subset of metastatic genes that encodes signaling molecules and membrane-anchored proteins capable of triggering robust

bone metastatic activity when simultaneously overexpressed was identified. This gene signature was ineffective in inducing cell homing activity to bone and local tumor growth but functionally contributed *in vivo* to induce aggressive tumoral bone colonization as reflected by the overt tumor burden and the osteolytic lesions. These *in vivo* findings were also associated with a concomitant increase in osteoclastogenesis *in vitro*. Interestingly, tumor-stromal interactions partially modulated this novel prometastatic gene subset by a TGF-β–dependent mechanism and induced global metalloproteolytic activities *in vitro*. *In vivo* global inhibition of both mechanisms led to increased survival and stunted bone metastasis burden and osteolytic lesions. Thus, our findings support the notion that this novel molecular signature contributes to aggressive bone colonization by a mechanism involving the cooperative action of osteoclastic bone resorption and bone matrix metalloproteolytic degradation.

Materials and Methods

Animals and cell culture. Four-week-old athymic nude mice were purchased from Harlan and maintained under specific pathogen-free conditions. Murine stromal ST-2 cell line was a kind gift from Dr. Civitelli (Washington University, St. Louis, MO). The NCI-H460 [a large cell carcinoma (21)] and SK-MES-1 (a human squamous cell carcinoma) cell lines were a kind gift from Dr. Gazdar (University of Texas Southwestern, Dallas, TX). All cell lines were maintained in RPMI 1640 supplemented with 10% fetal bovine serum.

Microarray data analysis: normalization, signal calculation, significant differential expression, and sample/gene profile clustering. Microarray data analysis was performed using the strategy and methods described elsewhere (22). Briefly, the robust microarray analysis (RMA) algorithm was used for background correction, intra- and inter-microarray normalization, and expression signal calculation (23–25). Once the absolute expression signal for each gene (i.e., the signal value for each probe set) was calculated in each microarray, a method [called significance analysis of microarray (SAM); ref. 26] was applied to calculate significant differential expression and find the gene probe sets that characterized the highly metastatic samples. The method uses permutations to provide robust statistical inference of the most significant genes and provides *P* values adjusted to multiple testing using false discovery rate (FDR; ref. 27). The main test was done by contrast of four control samples versus nine highly metastatic samples. However, having three different metastatic lines (M1, M4, and M5) done in triplicate, multiple SAM analyses were performed to find the genes showing significant differential expression that were also stable in different SAM tests. A cutoff of FDR < 0.20 was used for all the differential expression calculations. We applied all these methods using R[5] and Bioconductor.[6] Following the identification of differentially expressed gene probe sets, the corresponding matrix of expression values for all microarray hybridizations was analyzed using the "hclust" clustering algorithm implemented in R. This algorithm performs hierarchical cluster analysis with complete linkage to find similarity between probe sets based on their expression values in different chip microarrays analyzed. The algorithm classifies the probe sets in correlated groups presenting similar expression profiles or expression signatures. This overall strategy allowed the selection of key significant genes with similar expression profiles.

Global matrix metalloproteinase activity. Global matrix metalloproteinase (MMP) activity was measured in coculture supernatants using an assay based on the cleavage of a synthetic fluorogenic peptides as detailed in Supplementary Methods.

Metastasis assays. Intracardiac (i.c.) inoculation was performed as previously described (28). For intratibial (i.t.) injections, cultured cells (50–60% confluence) were harvested after a brief exposure to 0.25% trypsin and 0.02% EDTA, washed once in serum-free medium, and resuspended in PBS. Only single-cell suspensions with >95% viability were used for injections. Mice were anesthetized and the overlying skin over the proximal tibia and tibiofemoral region was prepped with betadine and 70% ethanol. A 2-mm longitudinal incision was performed over the patellar ligament with sterile scalpel, and a 1- to 2-mm longitudinal incision was made along the border of the ligament to the tibial plateau. Cells were injected (2.5×10^5 per mouse) in a total volume of 5 μL with a 29-gauge Hamilton microsyringe into the right tibia of anesthetized mice (eight mice per group). The contralateral tibia used as control was injected with the same volume of vehicle. Wounds were closed with a single 5-0 Vicryl suture. The experiment was ended 14 d after injection.

Statistical analysis. Log-rank test was used to calculate the statistical significance (*P* value) of differences observed among Kaplan-Meier curves. To study differences in proliferation rates, tumor growth, differences in metastatic area, number of osteoclasts, single-cell–derived colony (SCC) number, and metalloproteolytic activity data were analyzed by Kruskal-Wallis test with Dunn's multiple comparison test. Values were expressed as means ± SE and statistical significance was defined as $P < 0.05$ (*), $P < 0.01$ (**), and $P < 0.001$ (***). Supplementary Methods provide additional information.

Results

Development of highly metastatic cell lines with specific bone tropism. A systematic strategy was used to develop different models of NSCLC with bone tropism (data not shown). Cell lines were stably transfected with a luciferase reporter gene and their metastatic activity was assessed using *in vivo* bioluminescence imaging. During screening, one of the cell lines, NCI-H460, induced the most prominent bone metastases lesions in the hind limbs with short period of latency (Supplementary Table S1). Other sites include the spine and the forelimbs (Fig. 1*A*). To investigate whether these lesions were caused by an increase in bone resorption, tartrate-resistant acid phosphatase (TRAP) staining was performed to reveal the presence of osteoclasts. At the interface between the bone marrow and the endosteal surface of the diaphysis, the number of multinucleated TRAP-positive osteoclasts per bone interface was significantly increased in tumor-inoculated animals (Fig. 1*A*).

Next, subpopulations of cells with high metastatic ability were isolated following a previously described strategy (29). Briefly, after i.c. injection of H460 control cells, the subpopulations metastasizing with a high efficiency to bone were isolated and metastatic activity for each one was assessed by i.c. reinoculation of 10 mice per group. With some subpopulations, bone metastases appeared with a latency time ranging from 9 to 15 days to 20 to 30 days as assessed by X-ray imaging. Parallel monitoring revealed strong quenching of the luciferase reporter gene activity after two *in vivo* passages probably due to strong promoter methylation. This finding precluded the use of this technique to assess the metastatic activity. To circumvent this obstacle and to be able to systematically and accurately discriminate the subpopulations with different metastatic activities, three complementary variables were evaluated. First, metastatic activity of the injected control cells and all derived cellular subpopulations was assessed using Kaplan-Meier curves. Compared with the control cell line, several subpopulations, named M1, M4, and M5, had an increased metastatic activity by thriving efficiently at bone and decreasing animal survival (Fig. 1*A*). Second, 22 days after inoculation, computerized image analysis revealed an increased bone metastatic area of the hind limbs induced by the more aggressive subpopulations M1, M4, and M5 compared with the control cell line (Fig. 1*B*). And third, 22 days after i.c. inoculation, metastatic

[5] http://www.r-project.org
[6] http://www.bioconductor.org

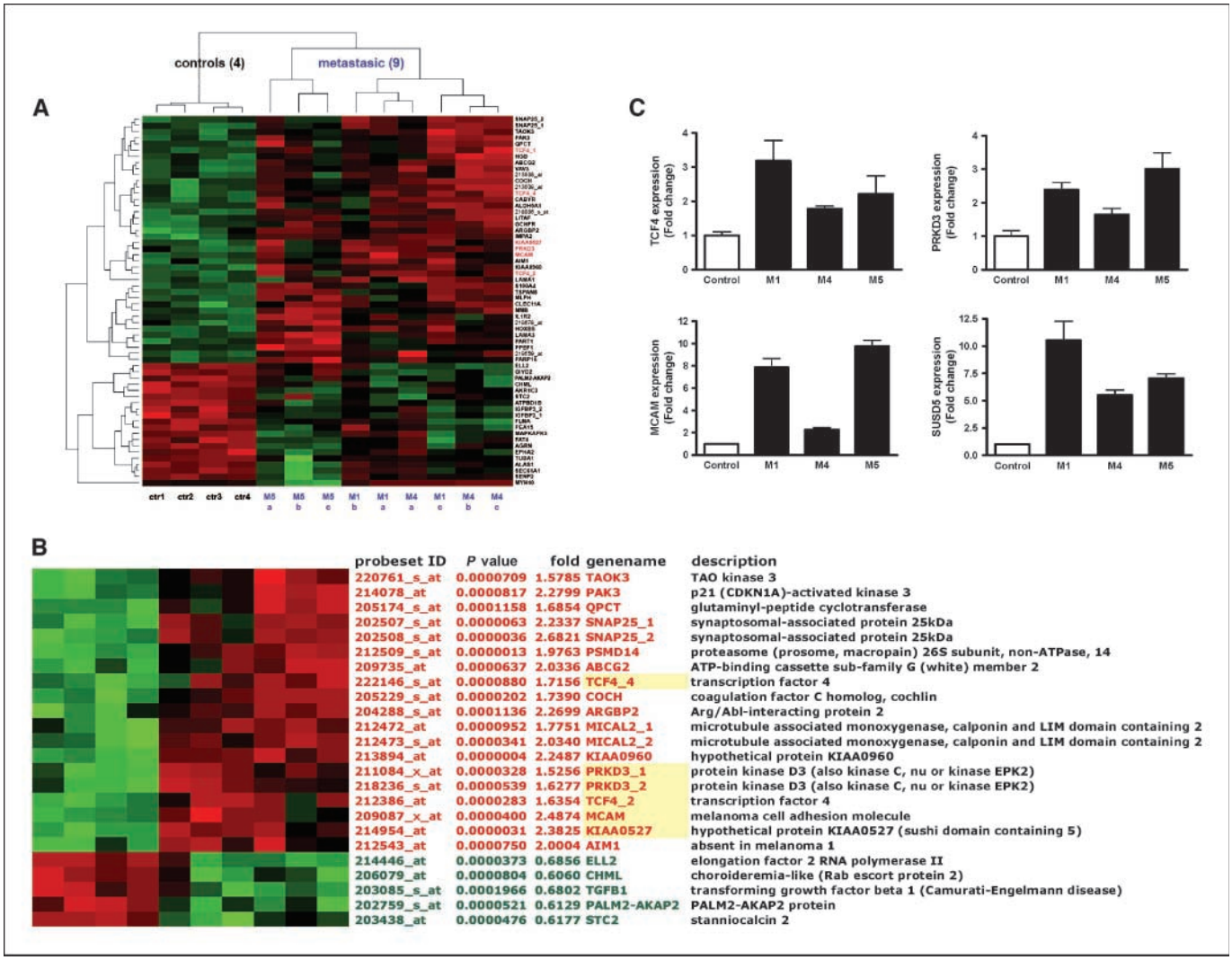

Figure 2. Metastasis gene signature. *A,* hierarchical cluster diagram of differentially expressed genes in control cell lines and the highly metastatic M1, M4, and M5. *B,* detailed list of the top statistically significant overexpressed and repressed genes. *Horizontal rows,* single-gene probe sets; *vertical columns,* results from the single-microarray hybridizations. Each box is the hybridization signal value of a gene probe set in the microarray assay. The intensity of the color saturation in each probe set box (ranging from 2 to 14 in log 2 scale) provides a quantitative estimation of its expression level (*red*, overexpression; *green*, repression). *C,* qPCR of four selected genes in the metastatic (*M1, M4,* and *M5*) versus control cells showing higher levels of expression of the four selected genes.

cells in the hind limbs were isolated by bone marrow "flushing." Conspicuous SCCs derived from each animal (10 mice per group) were counted. Subpopulations M1, M4, and M5 induced a more abundant yield of SCCs than control cell line (Fig. 1*C*). In contrast, other isolated subpopulations (M2, M3, M7, and M9), although weakly metastatic, showed no statistical differences with the control cell line in the Kaplan-Meier curves and SCCs (Supplementary Fig. S1). The number of osteoclasts per bone surface at the tumor-bone interface and the number of lesions in the hind limbs of animals inoculated with highly metastatic subpopulations did not reach statistical significance (Supplementary Fig. S1). To exclude the possibility of a cell autonomous growth effect, an *in vitro* proliferation assay was performed. Parental and derived M1, M4, and M5 displayed identical *in vitro* growth. Moreover, the highly metastatic cell lines formed s.c. tumors that grew at rates similar to control cells (Fig. 1*D*). Taken together, these data indicate that the M1, M4, and M5 subpopulations displayed a higher metastatic activity than the control H460 cell line. The metastatic ability observed *in vivo* was due to the acquisition of a bone metastatic phenotype, which presumably entailed an increased ability of homing and colonization that led to the formation of aggressive bone lesions.

Gene expression profile associated with bone metastasis. Next, we interrogated human microarrays to discriminate genes involved in metastatic behavior of highly metastatic subpopulations compared with parental and control luciferase-transfected cells. Gene expression signals were obtained by performing RMA (23). Figure 2*A* represents the clustering analysis based on a comparison between metastatic samples and controls, whereas a more stringent analysis was performed in Fig. 2*B*. Two of the four genes fulfilling the selection criteria encode for intracellular components: *TCF4* (*transcription factor 4, ITF-2, E2-2*), which encodes one of the four members of mammalian class I bHLH proteins, and *PRKD3* (*PKCν*), a serine-threonine kinase belonging to the Ca^{2+}/calmodulin-dependent protein kinase family, which has been implicated in the regulation of the cell signaling, proliferation,

migration, and apoptosis (30). Another identified gene was *MCAM* (*CD146, MUC18*), which encodes for a cell surface receptor belonging to the immunoglobulin superfamily involved in calcium-independent adhesion; it has been previously associated with melanoma cancer metastasis (31). A novel gene was also identified: *SUSD5* (*KIAA0527*), a "link domain" superfamily protein containing putative hyaluronic acid–binding domains. A complete list of the identities of these genes can be found in Supplementary Fig. S2. The results were confirmed using real-time quantitative PCR (qPCR; Fig. 2*C*).

Prometastatic gene signature. To investigate the contribution of TCF4, PRKD3, MCAM, and SUSD5 to the metastatic

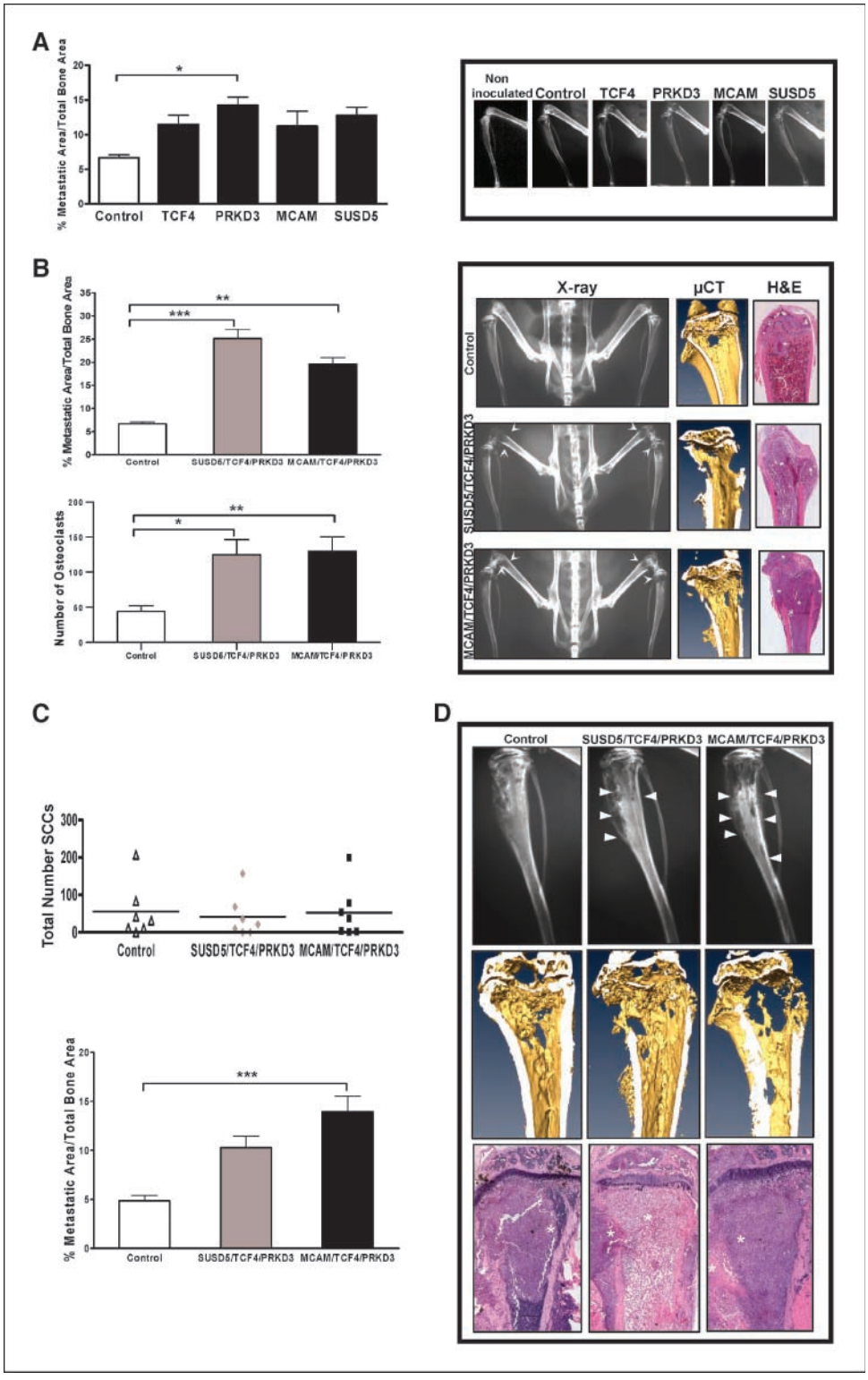

Figure 3. Delineation of functional metastatic properties of the gene signature. Single (*A*) or triple (*B–D*) overexpressors were i.c. inoculated (*A–C*) or i.t. injected (*D*). Twenty-two days after inoculation, the hind limbs were analyzed. *A,* histogram of the X-ray image analysis (*left*) and representative images (*right*) of hind limbs from mice inoculated with cells transduced with single overexpressors. *B,* histogram of X-ray image analysis of the metastatic area of the hind limbs of inoculated animals with control versus triple gene-bearing cells. Representative X-ray images, μCT scans of tibiae, and H&E staining. Mice inoculated with triple overexpressors had a strikingly similar tumor burden in both femora and tibiae of the same animal, a lack of trabecular bone in the primary spongiosa, and massive tumor colonization invading the bone marrow compartment. *Asterisk,* presence of tumor cells. *Bottom,* the number of TRAP-positive multinucleated cells at the tumor-bone interface in the long bones of animals inoculated with control and triple overexpressors was counted. *C,* 6 d after i.c. inoculation of the cells (control and triple overexpressors), the mice (seven mice per group) were sacrificed, cells were isolated from the hind limbs and allowed to grow for 5 d in selection medium, and all SCCs were counted. No differences were found among the groups. *D, in vivo* bone colonization of cells injected into the right tibia. *Bottom,* computerized X-ray image analysis shows dramatic differences 14 d after injection. Representative images of X-rays (*top*), μCT scans (*middle*), and H&E-stained tibial sections (*bottom*). Note the presence of bone marrow and cortical bone in the control animals. X-ray imaging shows higher bone metastatic area in the triple overexpressor–injected animals. H&E-stained femur sections show massive tumor colonization of the mice injected with triple overexpressors compared with control-injected animals. *Asterisk,* tumor-invaded area. *Columns,* mean of eight mice per group; *bars,* SE. *, $P < 0.05$; **, $P < 0.01$; ***, $P < 0.001$.

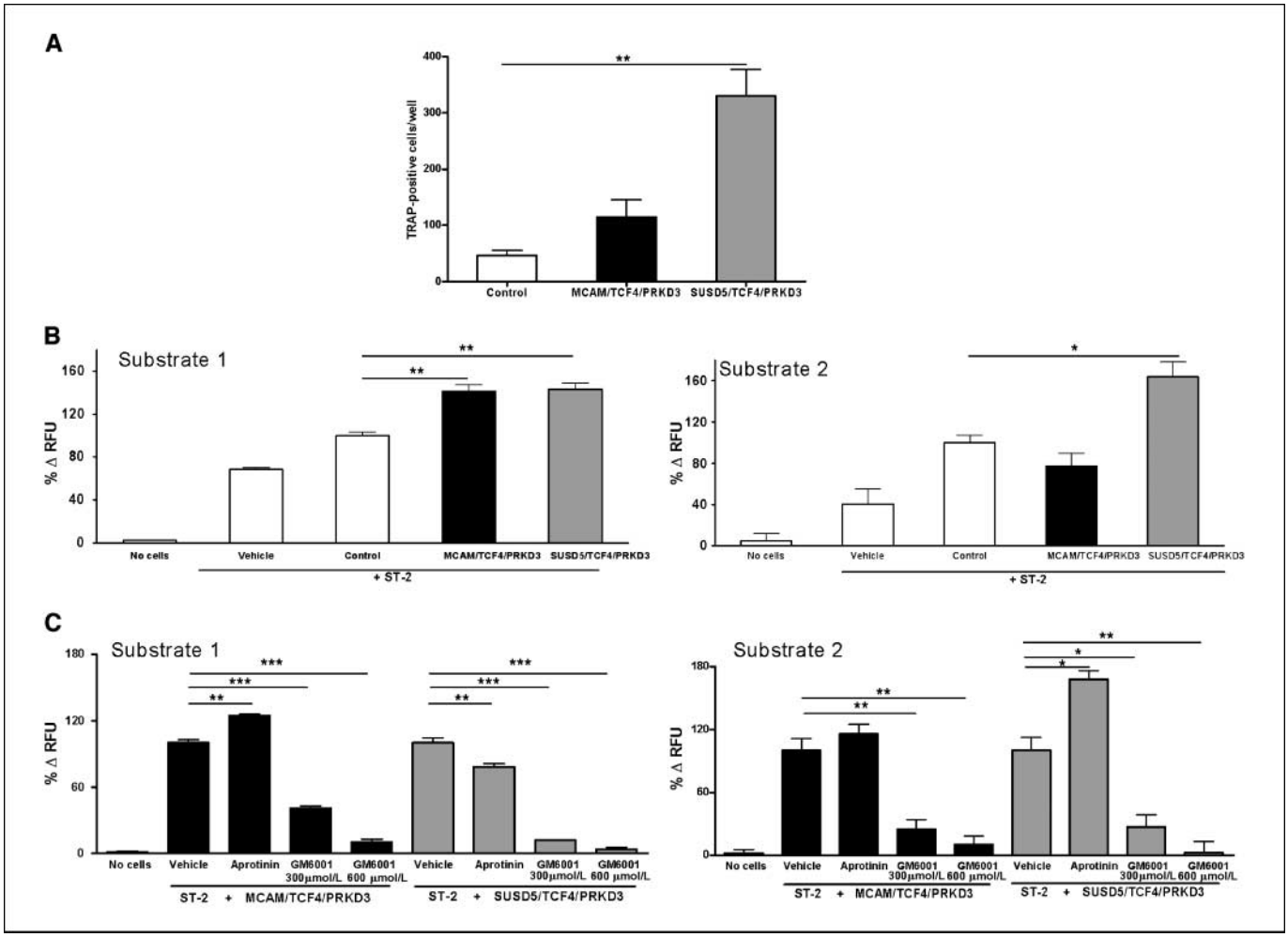

Figure 4. Metastatic signature induces metalloproteolytic and osteoclastogenic activities *in vitro. A, in vitro* osteoclastogenic assay. Conditioned media from control and triple combination cells were collected and then incubated with murine bone marrow macrophages for 6 d in macrophage colony-stimulating factor (20 ng/mL)–containing medium and receptor activator of nuclear factor-κB (40 ng/mL)–containing medium. In this assay, the conditioned medium of triple overexpressors induced the highest numbers of TRAP-positive multinucleated cells. The experiment was repeated thrice with identical results. *B,* global MMP activity in the conditioned medium of the triple overexpressors in coculture with ST-2 cells for 3 d assessed by digestion of fluorogenic substrates 1 (*left*) and 2 (*right*). *C,* inhibition of MMP activity using fluorogenic substrates 1 (*left*) and 2 (*right*) assessed in coculture medium from ST-2 and triple combination cells after incubation with a global MMP inhibitor, GM6001, or aprotinin (a non-MMP protease inhibitor). *Columns,* mean; *bars,* SE. *, $P < 0.05$; **, $P < 0.01$; ***, $P < 0.001$.

ability, pools of retrovirally transduced parental cells with single and triple gene combinations were generated and expression levels were measured by qPCR (Supplementary Fig. S3). To assess their metastatic activity, mice (eight mice per group) were i.c. inoculated with each simple and triple combinations. Compared with the control, cells overexpressing PRKD3 showed a significant increase ($P < 0.05$) in their ability to form metastasis (Fig. 3*A*). Interestingly, the triple gene combinations of SUSD5/TCF4/PRKD3 and MCAM/TCF4/PRKD3 showed a dramatic increase in the tumor burden as assessed by X-ray image analyses compared with control cells (Fig. 3*B*). Moreover, the number of osteoclasts per bone surface at the tumor-bone interface was significantly increased in animals inoculated with triple overexpressors (Fig. 3*B*). Of note, these effects were not due to enhanced proliferation because cell growth kinetics were unaltered both *in vitro* and *in vivo* (Supplementary Fig. S4). These data indicated that the triple gene combinations cooperatively promoted higher metastatic activity and enhanced the tumor burden and osteolytic lesions.

Cell homing effects and tumor colonization *in vivo*. To test whether the increase in metastatic lesions was due to a higher number of metastatic tumor cells that survived in bone, mice (seven mice per group) were injected with triple overexpressors and vector-transduced control cells. In preliminary experiments, it was established that, as early as 48 h after inoculation, a few cells (<10) could be isolated from the bone compartment of the hind limbs. To minimize variations due to the number of circulating cells during 3 to 4 days after inoculation, a surrogate measure of cell homing and survival activity was established by isolating all cells allocated in the bone compartment of the hind limbs at day 6 after inoculation. In preliminary experiments, any circulating cells were isolated at this time (data not shown). As shown in Fig. 3*C*, the number of isolated SCCs was strikingly similar among the groups, suggesting that the overexpressed genes did not affect the number of cells homing to bone. Next, the contribution of the metastatic signature to cell growth and colonization within the osseous compartment was assessed by i.t. injection. Triple gene combinations of SUSD5/TCF4/PRKD3 induced an increase in tibial

bone metastatic area and tumor burden (Fig. 3*D*), whereas the triple combination MCAM/TCF4/PRKD3 induced a more dramatic metastatic activity ($P < 0.001$). However, i.t. injection of triple transductants did not induce any changes in the number of tumor-derived osteoclasts (data not shown). These data indicate that these genes cooperatively contributed to enhance bone colonization, which led to an increased tumor burden.

TGF-β modulation of the metastatic profile and its regulation by tumor-stromal interactions. Bone is a major reservoir of several growth factors, including TGF-β, which is actively secreted by cells of the osteoblast lineage and stromal cells (20). Incubation of H460 cells with TGF-β increased TCF4, PRKD3, and SUSD5 levels by qPCR after 24 h, whereas MCAM levels were decreased (Supplementary Fig. S5*A*). No effects were observed in *in vitro* proliferation of triple overexpressors by exposure to TGF-β1 or p17 inhibitor (Supplementary Fig. S5*B*). Triple overexpressing cells were able to induce aggressive growth in the osseous compartment but not in s.c. derived tumors, suggesting that a site-specific metastatic genetic program highly dependent on the bone microenvironment was required. To mimic tumor-stromal interactions, H460 cells were cocultured with murine stromal ST-2 cells. Under these conditions, TCF4 and SUSD5 expression levels were markedly up-regulated, whereas a specific anti–TGF-β p17 peptide significantly decreased their expression levels. These data suggest that TGF-β released in the conditioned medium by H460 and ST-2, and/or stimulated by cell-cell interactions acting in

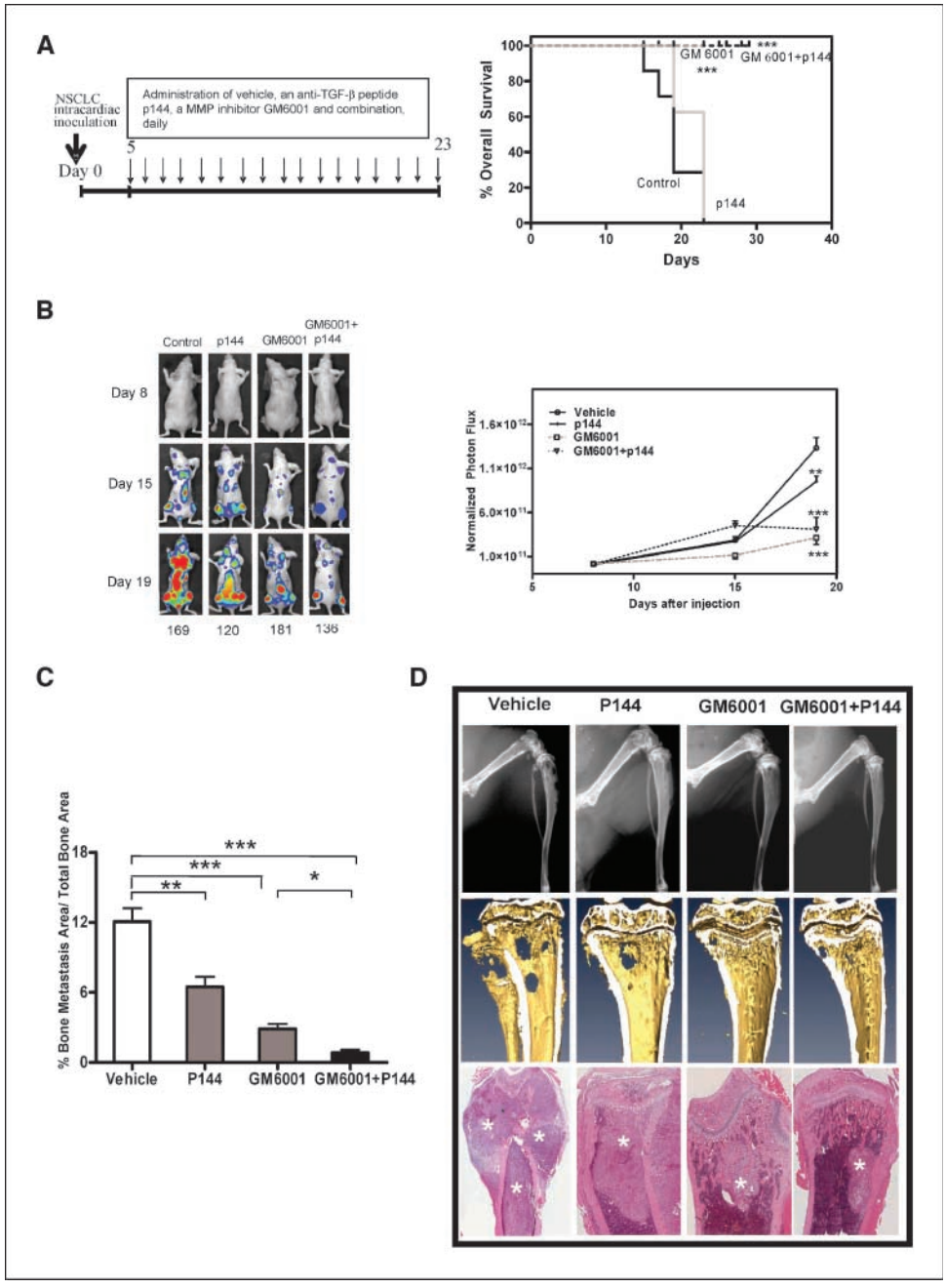

Figure 5. Pharmacologic inhibition of metalloproteolytic and osteoclastogenic activities impairs bone metastasis progression. *A,* therapeutic regiment (*left*) of mice treated with vehicle, anti–TGF-β (p144), GM6001, or combination and Kaplan-Meier curves (*right*) showing the overall survival of different treated groups. *B,* bioluminescence imaging showing slow progression of lesions in treated animals compared with controls. *Left,* representative images; *right,* quantification of normalized photon flux. **, $P < 0.01$; ***, $P < 0.001$, based on rank sum test compared with control at the last time point. *C,* computerized image analysis of X-rays obtained from all animals revealed a decreased metastatic area in treated animals compared with vehicle control mice. *Columns,* mean of seven mice per group; *bars,* SE. *, $P < 0.05$; **, $P < 0.01$; ***, $P < 0.001$, calculated using the rank sum test with Bonferroni adjustment. *D,* representative X-ray images (*top*), three-dimensional reconstruction of μCT scans (*middle*), and H&E staining (*bottom*). *Asterisk,* presence of tumor cells.

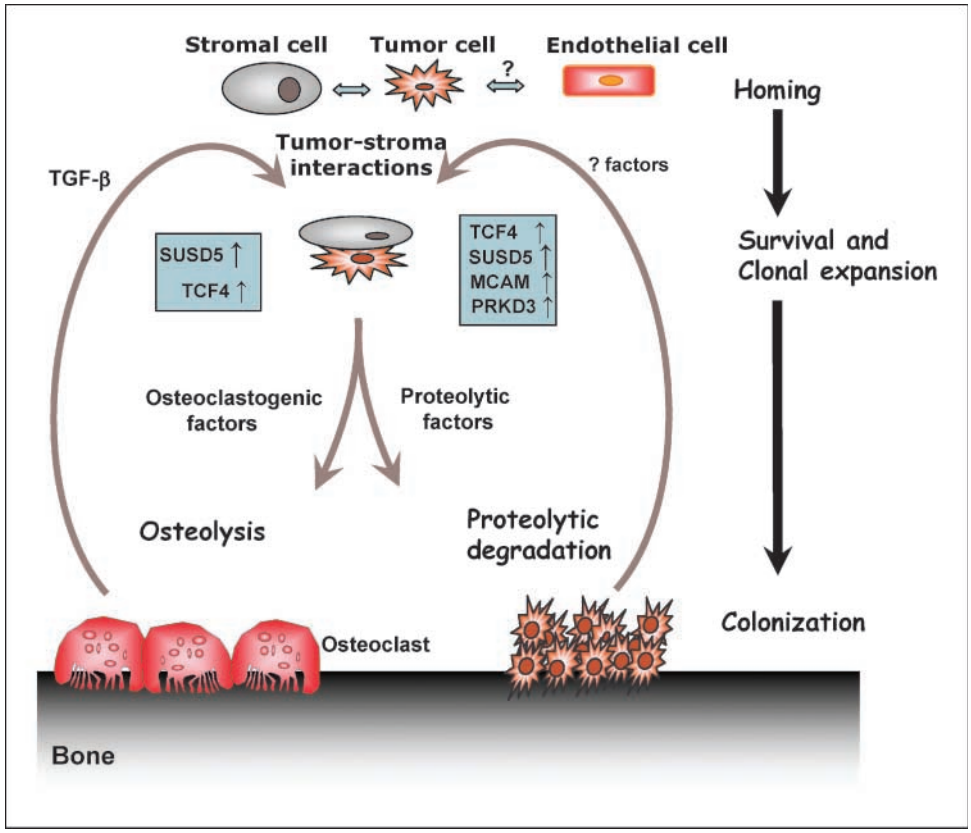

Figure 6. Model of tumor-bone colonization within the osseous microenvironment. A schematic model representing tumor-bone colonization in which a subset of genes allows tumor cells to thrive in the bone compartment. Stringent selection process at the primary tumor would endow cells with advantageous functions driven by a subset of genes favoring osseous colonization but not affecting the number of cells homing to bone. During the initial steps of bone homing, two events were consistently present in our model. First, a limited number of metastatic precursors were found in bone after i.c. inoculation, suggesting the inefficiency of the osseous cell homing process. Second, metastases were regularly located within the metaphysis of long bones, both in the primary spongiosa and in the periosteum of the femorotibial region. Rather than occurring as a result of stochastic events, the uniform location of these lesions argues in favor of a model where specific tumor endothelial engagement and/or mechanical constraints imposed by the osseous microvascular bed in the periosteum and the primary spongiosa would allow cell arrest and survival. Complementary to this view, either growth within the capillaries or the extravasation of the cells into the bone compartment would result in modulation of the gene signature by complex tumor-stromal interactions and bone matrix–derived factors exacerbating osteoclast resorption and enhancing proteolytic activity. Our experimental evidence establishes the proof of concept that double inhibition of these mechanisms may be required to effectively impair metastasis.

autocrine/paracrine manner, was partially mediating these effects (Supplementary Fig. S5*C*). No differences were found for PRKD3 and MCAM.

Mechanisms of bone matrix degradation. To investigate the mechanism accounting for the higher number of osteoclasts found after i.c. inoculation of triple overexpressors in bone metastatic lesions *in vivo*, we determined whether the metastatic signature could induce tumor-derived osteoclastogenic factors *in vitro*. Compared with control cells, conditioned medium from SUSD5/TCF4/PRKD3 induced strong osteoclastogenic activity in an assay of murine bone marrow macrophages ($P < 0.01$; Fig. 4*A*). Of note, the levels of PTHrP and the strong osteoclastogenic cytokine interleukin-8 (IL-8) were unaltered in triple transfectants and highly metastatic subpopulations (M1, M4, and M5; Supplementary Fig. S6).

However, the increase in osteoclast number *in vitro* could not totally explain the aggressive osteolytic lesions induced *in vivo*, and therefore, other mechanisms of bone matrix degradation may exist. Similarly, the fact that after i.t. injection the aggressive bone colonization induced by the high tumor burden was not associated with high osteoclast number (see above) also suggested alternative mechanisms of osteolysis. In this regard, it is widely known that tumor stroma–derived MMPs represent a frequent mechanism of matrix degradation in many tumors. To explore this possibility, global MMP activity was assessed by a kinetic fluorescence assay under conditions that mimicked *in vivo* tumor-stromal interactions. Conditioned medium released by coculture of triple overexpressors with ST-2 cells induced a ~40% higher activity compared with control cells using a fluorogenic substrate 1 (preferentially cleaved by MMP-3 and MMP-10; $P < 0.01$). Similarly, using a substrate 2 (preferentially cleaved by MMP-2 and MMP-9), triple SUSD5/TCF4/PRKD3 incubated with ST-2 cell–conditioned medium induced ~60% higher activity ($P < 0.05$; Fig. 4*B*). The serine protease inhibitor aprotinin showed inhibitory activity or even stimulated the proteolytic activity present in the conditioned medium. In contrast, the global MMP inhibitor GM6001 completely abrogated the metalloproteolytic activity in a dose-dependent manner (Fig. 4*C*). However, an anti–TGF-β peptide (p17) did not have an effect on the global proteolytic activity in the same culture system (data not shown). These findings indicate that *in vivo* proteolytic bone matrix degradation could be partially mediated by a mechanism that involves one or several MMPs released by tumor cells and/or tumor-stromal interactions.

Involvement of TGF-β and MMP activities *in vivo*. Because tumor-stromal interactions increased *in vitro* expression levels of

several prometastatic genes by a TGF-β–mediated mechanism, we tested the contribution of TGF-β *in vivo*. In a preliminary experiment, mice were treated with a p17 anti–TGF-β peptide and compared with an irrelevant peptide (p41) and vehicle-treated animals (Supplementary Fig. S7). X-ray analysis revealed that p17 peptide decreased the tumor burden and the number of osteoclasts at tumor-bone interface compared with p41 and vehicle-treated animals ($P < 0.05$). Similar results were obtained by using an anti–TGF-β antibody (Supplementary Fig. S7). Of note, inhibition of the bone metastatic area was not completely abrogated, suggesting other mechanisms of bone matrix degradation independent of TGF-β.

Previous *in vitro* findings suggested that MMP activities could play a role in tumor-mediated bone degradation. Thus, we tested the extent to which TGF-β and global metalloproteolytic activities were mediating the detrimental effects of bone metastasis *in vivo*. We used the i.c. inoculation model to assess the efficacy of single or combined anti–TGF-β peptide (p144) and a broad-spectrum MMP inhibitor (GM6001). We use p144 because of its availability at the time of the experimental procedure. Both p17 and p144 have shown similar efficacy *in vivo* (32, 33). Highly metastatic M5 cells retrovirally transduced with a robust luciferase reporter gene were i.c. injected and treated daily according to the therapeutic regimen shown in Fig. 5*A*. Combined drug inhibition led to a significant increase in overall survival in animals treated with GM6001 and p144 compared with vehicle control (Fig. 5*A*). These results were correlated with a significant decrease in bone colonization on day 19 after inoculation as assessed by bioluminescence imaging (Fig. 5*B*). Inhibition by GM6001 alone or in combination markedly reduced tumor burden and significantly reduced metastatic lesions in seven of seven mice as assessed by X-ray image analysis and μCT (Fig. 5*C* and *D*). More importantly, the combination therapy reduced the metastatic area more than either single treatment alone. Histologic analysis of vehicle-treated animals revealed the complete colonization of the bone marrow compartment with destruction of cortical bone in the metaphyseal region and the colonization of extraosseous tissues. In contrast, p144 animals showed the presence of abundant colonization at the metaphysis and tumor cells located subperiostally at the metaphyseal region. GM6001 alone or in combination led to small isolated metastatic clones adjoining the primary spongiosa without affecting the trabecular bone in the metaphyseal region (Fig. 5*D*). Of note, anti–TGF-β p144 treatment alone decreased tumor burden by bioluminescence imaging ($P < 0.01$; Fig. 5*B*) and bone lesions by X-ray imaging ($P < 0.01$; Fig. 5*C* and *D*), whereas this peptide did not have any effect in overall survival. More importantly, the combination therapy reduced the metastatic area more than each single treatment alone. Taken together, these data indicated that blockade of TGF-β and MMP activities remarkably attenuated the development of bone metastatic lesions by severely decreasing the metastatic burden and osteolytic lesions and markedly increasing overall survival.

Discussion

Lung cancer patients who develop osseous metastases have a high morbidity and a poor prognosis. To date, the mechanisms of lung cancer dissemination and colonization of bone have been poorly understood. This report presents a xenograft model of large cell carcinoma, the most lethal lung cancer subtype in humans. In this model, tumor cells induce selective, rapid, and reproducible bone metastases. Transcriptomic analysis identified a novel gene signature that was implicated in the high prometastatic activity leading to overt osseous colonization. This subset of genes allowed tumor cells to thrive in the bone compartment by inducing bone matrix degradation, which was accomplished by concurrent osteoclastic resorption and metalloproteolytic release. Pharmacologic inhibition of both activities was effective at abrogating bone metastasis and increasing survival.

The present study identified functional interactions among this subset of genes that cooperatively mediated bone colonization. With the exception of MCAM, which is involved in melanoma progression and metastasis (34), this functionally validated transcriptomic signature entails genes that have not been previously implicated in metastasis. The other genes include *TCF4*, which is a downstream target of the Wnt/β-catenin/TCF pathway (35). Interestingly, TCF4 is active during lung morphogenesis, and this conserved molecular key cascade has also been implicated in lung cancer (36). Another signaling molecule, PRKD3 belongs to a family of proteins participating in a variety of key cellular processes related to metastasis, including cell motility, invasion, adhesion, and oxidative stress (reviewed in ref. 30). Interestingly, PRKD3 and TCF4 overexpression alone or in combination elicited marked prometastatic activity, which suggests novel roles for these proteins in carcinogenesis. Finally, the other previously unidentified component of our metastatic signature, SUSD5 is structurally related to a protein superfamily containing hyaluronic acid–binding domains. This family includes extracellular matrix proteins and membrane receptors, such as CD44, which are involved in multiple functions, such as tumor cell adhesion, proliferation, migration, and invasion (reviewed in ref. 37).

These results agree with previous studies dealing with breast cancer, where multiple genes were found to complement each other to fulfill several necessary functions for the development of the metastatic phenotype (29). These findings may also reflect that the minimum set of functions required for bone homing and colonization could be performed by different gene combinations. Of note, none of the genes from the breast metastatic signature was shared by our transcriptomic profile, although both studies found identical bone tropism and noted similarities in the mechanism of the osteoclastic lesions. One would expect at least some degree of redundancy in the biological functions of both gene signatures. One possible explanation for this apparent discrepancy is the fact that the breast and lung cancer cell lines have different metastatic activities, incidence, and latency. Breast MDA-MB-231 cells induced more indolent metastasis (~40% of mice developed metastases 140 days after inoculation according to ref. 29) compared with the aggressive lung H460 parental cells (~50% of the animals 35 days after inoculation). This striking divergence suggests different activities in the bone colonization mechanisms; this may reflect the subset of identified genes and their biological activities. Furthermore, this may explain that an active signaling molecule, such as PRKD3, was easily selected in the lung cancer transcriptomic signature and by itself was able to promote strong bone colonization. In contrast, in the breast metastasis model, the less biologically active proteins required the combination with the multifunctional bone matrix protein osteopontin to promote strong metastatic activity (29).

About the mechanism of osteolysis in the breast cancer model, osteoclast activity was mediated by tumor-derived PTHrP (17, 19) and IL-8 (38), increasing osteoclast resorption. This effect was further exacerbated by bone-derived TGF-β (12, 20). In contrast, in the present model, the *in vitro* expression levels of PTHrP and

IL-8 were similar among the triple overexpressors, the highly metastatic subpopulations, and control cell lines (Supplementary Fig. S6). Thus, these results raise the intriguing possibility that, in addition to these osteoclastogenic molecules (39), other unidentified factors, perhaps downstream target genes of the metastatic gene signature, might be involved in tumor-derived osteoclast activation.

These findings also support the involvement of TGF-β in a common mechanism of bone metastasis, modulating the prometastatic gene signature and exacerbating tumor-induced osteolysis. In breast and renal carcinoma (17, 18), a specific TGF-β signaling blockade of tumor cells was achieved by a dominant-negative strategy, in contrast to the systemic inhibition in the present model. Although both methods were successful in attenuating bone metastasis, global inhibition may have additional beneficial effects in an immunocompetent model by further enhancing the immune response because TGF-β contributes to the evasion of tumor cell immunoreactivity (40). Although this hypothesis needs to be validated, the chronic administration of anti–TGF-β modalities is compatible with long-term survival in metastases (41).

Our findings underscore the role of cell autonomous effects mediated by a subset of genes whose intrinsic concurrent overexpression was required for the secretion of a complex of MMPs that resulted in elevated proteolytic activity. Previous studies in early stages of lung cancer revealed the diversity of MMPs, which was correlated with a poor prognosis (42). Interestingly, in the present study, the proteolytic activity *in vitro* may have resulted from the net balance of a complex of different proteases and their natural inhibitors because the MMPs able to degrade the fluorogenic substrate assay include MMP-1, MMP-2, MMP-3, MMP-9, and MMP-10. It is important to note that our *in vitro* coculture system does not fully reconstitute the complexity of the *in vivo* tumor-bone interface where other cells could potentially contribute to the increase in extracellular proteolytic activity. For instance, osteoclast-released MMP-7 is a major contributor to cancer-induced osteolysis in a prostate metastasis model (43). Additional osteoclast-derived enzymes, such as cathepsin K and other MMPs released by osteoclasts, could also participate in this process. This mechanism triggers aggressive proteolytic degradation at the tumor-bone interface, as suggested by the i.t. injection experiment and in lesions induced by the highly metastatic M5 subpopulation where osteoclast numbers were low due to the lack of availability of marrow progenitors or a compromised blood supply. Thus, this mechanism may prevail in advanced lesions with an elevated tumor burden, whereas in the early stages tumor release factors produced by metastatic cells may facilitate the progressive induction of a high number of osteoclasts driving this primary mechanism of bone destruction.

In addition to cell autonomous effects, several findings highlight the role of host-derived functions in modulating the development of metastases. First, two prometastatic components of our gene signature, SUSD5 and TCF4, were strongly up-regulated in the coculture system. Second, tumor-stromal interactions of triple overexpressors were required to induce strong proteolytic activity *in vitro*. Third, this effect was bone specific because it was associated with a dramatic increase in the bone tumor burden and osteolytic metastasis *in vivo*, although s.c. growth was unaffected. These findings agree with the "seed and soil" hypothesis (7) and support the notion that each tissue imposes different requirements that are highly dependent on tumor-stromal interactions for promoting metastatic growth.

In summary, a genetic transcriptomic profile identified several genes that cooperatively mediated metastatic osseous colonization by favoring strong osteoclastogenic effects as well as high metalloproteolytic activity. Thus, we suggest that effective pharmacologic inhibition of bone destruction may require targeting both arms of osteolytic degradation: the tumor-induced osteoclast resorption and the deleterious proteolytic action triggered at tumor-stromal interface (Fig. 6).

Acknowledgments

Received 12/4/2007; revised 1/9/2008; accepted 1/29/2008.

Grant support: "UTE project FIMA" agreement, RTICCC C03/10, ISCIII-RETIC RD06/0020, ISCIII-FIS PI042282, FIT-090100-2005-46, "Ortiz de Landázuri" grant 67/2005 (Government of Navarra), "La Caixa Foundation," and "FMMA" awards (F. Lecanda); ISCIII-FIS PI061153 and Castilla-Leon Government grant CSI03A06 (J. De Las Rivas); Royo Foundation (S. Vicent); FIMA and FPU (D. Luis-Ravelo); and Basque Government (I. Antón). F. Lecanda is an investigator from the "Ramón y Cajal" and I3 Programs.

The costs of publication of this article were defrayed in part by the payment of page charges. This article must therefore be hereby marked *advertisement* in accordance with 18 U.S.C. Section 1734 solely to indicate this fact.

We thank S. Martínez, C. Zandueta, A. Urbiola, and D. Pérez for their outstanding technical assistance.

References

1. Jemal A, Tiwari RC, Murray T, et al. Cancer statistics, 2004. CA Cancer J Clin 2004;54:8–29.
2. Tuveson DA, Jacks T. Modeling human lung cancer in mice: similarities and shortcomings. Oncogene 1999;18:5318–24.
3. De Stefani E, Deneo-Pellegrini H, Boffetta P, et al. Cigarette smoking and risk of large cell carcinoma of the lung: a case-control study in Uruguay. Lung Cancer 2004;43:267–74.
4. Blanchon F, Grivaux M, Asselain B, et al. 4-Year mortality in patients with non-small-cell lung cancer: development and validation of a prognostic index. Lancet Oncol 2006;7:829–36.
5. Fry WA, Menck HR, Winchester DP. The National Cancer Data Base report on lung cancer. Cancer 1996;77:1947–55.
6. Ginsberg RJ, Kris MG, Armstrong JG. Non-small cell lung cancer. Philadelphia: Lippincott Williams and Wilkins; 2001. p. 673–713.
7. Paget S. The distribution of secondary growths in cancer of the breast. Lancet 1889;1:571–3.
8. Mohla S, Weilbacher KN, Cher ML, Oyajobi BO, Poznak CV, Clohisy DR. Third North American Symposium on Skeletal Complications of Malignancy: summary of the scientific sessions. Cancer 2003;97:719–25.
9. Coleman RE. Skeletal complications of malignancy. Cancer 1997;80:1588–94.
10. Delea T, Langer C, McKiernan J, et al. The cost of treatment of skeletal-related events in patients with bone metastases from lung cancer. Oncology 2004;67:390–6.
11. Dumont N, Arteaga CL. Targeting the TGFβ signaling network in human neoplasia. Cancer Cell 2003;3:531–6.
12. Mundy GR. Metastasis to bone: causes, consequences and therapeutic opportunities. Nat Rev Cancer 2002;2:584–93.
13. Massague J, Blain SW, Lo RS. TGFβ signaling in growth control, cancer, and heritable disorders. Cell 2000;103:295–309.
14. Derynck R, Akhurst RJ, Balmain A. TGF-β signaling in tumor suppression and cancer progression. Nat Genet 2001;29:117–29.
15. Kang Y, He W, Tulley S, et al. Breast cancer bone metastasis mediated by the Smad tumor suppressor pathway. Proc Natl Acad Sci U S A 2005;102:13909–14.
16. Deckers M, van Dinther M, Buijs J, et al. The tumor suppressor Smad4 is required for transforming growth factor β-induced epithelial to mesenchymal transition and bone metastasis of breast cancer cells. Cancer Res 2006;66:2202–9.
17. Kakonen SM, Selander KS, Chirgwin JM, et al. Transforming growth factor-β stimulates parathyroid hormone-related protein and osteolytic metastases via Smad and mitogen-activated protein kinase signaling pathways. J Biol Chem 2002;277:24571–8.
18. Kominsky SL, Doucet M, Brady K, Weber KL. TGF-β promotes the establishment of renal cell carcinoma bone metastasis. J Bone Miner Res 2007;22:37–44.

19. Yin JJ, Selander K, Chirgwin JM, et al. TGF-β signaling blockade inhibits PTHrP secretion by breast cancer cells and bone metastases development. J Clin Invest 1999; 103:197–206.

20. Guise TA, Yin JJ, Taylor SD, et al. Evidence for a causal role of parathyroid hormone-related protein in the pathogenesis of human breast cancer-mediated osteolysis. J Clin Invest 1996;98:1544–9.

21. Phelps RM, Johnson BE, Ihde DC, et al. NCI-Navy Medical Oncology Branch cell line data base. J Cell Biochem Suppl 1996;24:32–91.

22. Castellano E, De Las Rivas J, Guerrero C, Santos E. Transcriptional networks of knockout cell lines identify functional specificities of H-Ras and N-Ras: significant involvement of N-Ras in biotic and defense responses. Oncogene 2007;26:917–33.

23. Irizarry RA, Hobbs B, Collin F, et al. Exploration, normalization, and summaries of high density oligonucleotide array probe level data. Biostatistics 2003;4: 249–64.

24. Irizarry RA, Bolstad BM, Collin F, Cope LM, Hobbs B, Speed TP. Summaries of Affymetrix GeneChip probe level data. Nucleic Acids Res 2003;31:15.

25. Bolstad BM, Irizarry RA, Astrand M, Speed TP. A comparison of normalization methods for high density oligonucleotide array data based on variance and bias. Bioinformatics 2003;19:185–93.

26. Tusher VG, Tibshirani R, Chu G. Significance analysis of microarrays applied to the ionizing radiation response. Proc Natl Acad Sci U S A 2001; 98:5116–21.

27. Benjamini Y, Hochberg Y. Controlling the false discovery rate: a practical and powerful approach to multiple testing. J Roy Stat Soc 1995;57:289–300.

28. Gonzalez I, Vicent S, de Alava E, Lecanda F. EWS/FLI-1 oncoprotein subtypes impose different requirements for transformation and metastatic activity in a murine model. J Mol Med 2007;85:1015–29.

29. Kang Y, Siegel PM, Shu W, et al. A multigenic program mediating breast cancer metastasis to bone. Cancer Cell 2003;3:537–49.

30. Rozengurt E, Rey O, Waldron RT. Protein kinase D signaling. J Biol Chem 2005;280:13205–8.

31. Xie S, Luca M, Huang S, et al. Expression of MCAM/MUC18 by human melanoma cells leads to increased tumor growth and metastasis. Cancer Res 1997;57:2295–303.

32. Ezquerro IJ, Lasarte JJ, Dotor J, et al. A synthetic peptide from transforming growth factor β type III receptor inhibits liver fibrogenesis in rats with carbon tetrachloride liver injury. Cytokine 2003;22: 12–20.

33. Dotor J, López-Vázquez AB, JJ L, et al. Identification of peptide inhibitors of transforming growth factor β1 using a phage-displayed peptide library. Cytokine 2007; 39:106–15.

34. Mills L, Tellez C, Huang S, et al. Fully human antibodies to MCAM/MUC18 inhibit tumor growth and metastasis of human melanoma. Cancer Res 2002;62: 5106–14.

35. Kolligs FT, Nieman MT, Winer I, et al. ITF-2, a downstream target of the Wnt/TCF pathway, is activated in human cancers with β-catenin defects and promotes neoplastic transformation. Cancer Cell 2002;1:145–55.

36. You L, He B, Xu Z, et al. Inhibition of Wnt-2-mediated signaling induces programmed cell death in non-small-cell lung cancer cells. Oncogene 2004;23:6170–4.

37. Toole BP, Wight TN, Tammi MI. Hyaluronan-cell interactions in cancer and vascular disease. J Biol Chem 2002;277:4593–6.

38. Bendre MS, Margulies AG, Walser B, et al. Tumor-derived interleukin-8 stimulates osteolysis independent of the receptor activator of nuclear factor-κB ligand pathway. Cancer Res 2005;65:11001–9.

39. Iguchi H, Onuma E, Sato K, Ogata E. Involvement of parathyroid hormone-related protein in experimental cachexia induced by a human lung cancer-derived cell line established from a bone metastasis specimen. Int J Cancer 2001;94:24–7.

40. Thomas DA, Massague J. TGF-β directly targets cytotoxic T cell functions during tumor evasion of immune surveillance. Cancer Cell 2005;8:369–80.

41. Yang YA, Dukhanina O, Tang B, et al. Lifetime exposure to a soluble TGF-β antagonist protects mice against metastasis without adverse side effects. J Clin Invest 2002;109:1607–15.

42. Cho NH, Hong KP, Hong SH, Kang S, Chung KY, Cho SH. MMP expression profiling in recurred stage IB lung cancer. Oncogene 2004;23:845–51.

43. Lynch CC, Hikosaka A, Acuff HB, et al. MMP-7 promotes prostate cancer-induced osteolysis via the solubilization of RANKL. Cancer Cell 2005;7:485–96.